

Effect of H on the crystalline and magnetic structures of the $\text{YCo}_3\text{-H(D)}$ system. II. $\text{YCo}_3\text{-H(D)}_x$ from x-ray and neutron powder diffraction

Jian Liu, Xiang-Yuan Cui, Peter A. Georgiev, Ian Morrison, and D. Keith Ross

Institute for Materials Research, Joule Physics Laboratory, University of Salford, Salford, M5 4WT, United Kingdom

Mark A. Roberts

SRS, Daresbury Laboratory, Warrington, Cheshire, WA4 4AD, United Kingdom

Ken A. Andersen and Mark Telling

ISIS, Rutherford Appleton Laboratory, Chilton, Didcot, Oxfordshire OX11 0QX, United Kingdom

Dave Fort

School of Metallurgy and Materials, The University of Birmingham, Edgbaston, Birmingham, B15 2TT, United Kingdom

(Received 25 May 2007; published 30 November 2007)

The crystalline and magnetic structures of the $\text{YCo}_3\text{-H(D)}$ system have been investigated by means of x-ray and neutron diffraction with the objective of understanding the complex magnetic changes that are observed in this system as hydrogen is added. Synchrotron x-ray diffraction (XRD) patterns were first refined to yield the lattice parameters and coordination of Y and Co atoms in the metal and two β -hydride phases while XRD was used for the γ phase. *In situ* neutron powder diffraction measurements of YCo_3D_x were then made in all four phases to determine the deuterium site occupancies and magnetic structures. The site occupancies were also rationalized using the Westlake geometric model. The highest hydrogen concentration measured was $\text{YCo}_3\text{H}_{4.6}$. Using the Westlake model, we conclude that the saturated hydrogen content would be YCo_3H_5 . Our results reported here and in Part I [Phys. Rev. B 76, 184443 (2007)] have enabled us to rationalize the changes in the magnetic structures in terms of changes in the cobalt-cobalt distance caused by the addition of hydrogen. In particular, in the antiferromagnetic γ phase, we observe Co atomic displacements that enable the structure to adopt a particular antiferromagnetic structure in a manner that is reminiscent of a Peierls distortion as observed in transitions from the conducting to nonconducting hydrides on addition of hydrogen in YH_3 .

DOI: [10.1103/PhysRevB.76.184444](https://doi.org/10.1103/PhysRevB.76.184444)

PACS number(s): 75.50.Gg, 61.10.Nz, 61.12.Ld

I. INTRODUCTION

The YCo_3/H system is of considerable intrinsic interest because of the dramatic changes in magnetization that occurs as the hydrogen is added.¹ It is particularly interesting to investigate whether the changes in magnetic behavior are due predominantly to changes in the electronic density of states or due to changes in the separation of the various cobalt atoms. In Part I, we reported on *ab initio* calculations and neutron powder diffraction (NPD) studies of the magnetic structure of YCo_3 itself. In Part II of this study, we report accurate determinations of how the crystalline and magnetic structures evolve as deuterium is added. In a previous paper, we reported on *ab initio* calculations of the magnetic properties of YCo_3H_2 .²

YCo_3 alloy has two established hydride phases: the β and the γ phases. Yamaguchi *et al.*^{1,3} reported the dramatic influence of the hydrogen content on the magnetic properties of both Y_2Co_7 and YCo_3 . They showed the remarkable restoration of the magnetic moments within the wide hydrogen content range of the β phase, from antiferromagnetic (or paramagnetic) in the β_1 phase for the low hydrogen content side to ferromagnetic in the β_2 phase for the high hydrogen content side, while the γ phase is antiferromagnetic.^{1,3-5}

The crystal structures of the YCo_3 hydride phases have also been studied, by means of both x-ray and neutron diffraction. Benham *et al.*⁶ studied the crystal structures of

$\text{YCo}_3\text{D}_{1.0}$ and $\text{YCo}_3\text{D}_{1.9}$, and found that of the 13 possible types of interstitial site [as for HoNi_3 (Ref. 7)], only the $36i_1$ sites were filled in the AB_2 unit and that only the c lattice parameter was expanded, by about 10%. The refined position of the D atom corresponds to the center of a pair of $36i_1$ sites, so its coordinates are given as $18h(x, -x, z)$ site. Bartashevich *et al.*⁸ showed that, for the γ phase, in addition to the $36i_1$ site, the $18h_2$ and $36i_2$ sites in the AB_5 unit are partially filled, giving $\text{YCo}_3\text{D}_{3.8}$, and that the lattice now also expanded in the “ a ” direction.

In our recent research on the pressure-composition isotherms and magnetization of $\text{YCo}_3\text{-H}$, we identified an additional hydride phase of YCo_3 .⁹ At room temperature, a new phase transformation exists within the previously observed β -phase region. Hence the previous observation of the β_1 and β_2 magnetic behavior can be attributed to the different structures of these phases. The magnetization measurements confirmed that YCo_3 is ferrimagnetic, the β_1 hydride is paramagnetic, the β_2 hydride is ferromagnetic, and the γ hydride is antiferromagnetic.

In the present paper, we extend the previous work in various ways with a view to understanding the origins of the hydrogen-induced changes in magnetic structures: we investigate the structure of $\text{YCo}_3\text{D}_{1.3}$, typical of the β_1 phase, because, according to our measurements of composition-pressure isotherms,⁹ the previously reported $\text{YCo}_3\text{D}_{1.0}$ structure⁶ lies in the $(\alpha + \beta_1)$ two-phase region. We then in-

investigate the structural difference between the β_1 and the recently discovered β_2 hydride phase. We also investigate the deuterium occupancies in $\text{YCo}_3\text{D}_{4.6}$ (the γ phase) at the highest obtainable deuterium concentrations. All the structures have been refined with improved accuracy by combining high resolution synchrotron, XRD, and NPD data sets. This has enabled us to calculate the interstitial hole sizes and the separation between nearest-neighbor interstitial sites with improved accuracy. The Westlake geometric model^{10,11} can thus be used to rationalize the deuterium site occupancies in YCo_3D_x ($x=1.3, 2.0, \text{ and } 4.6$), and the saturated hydrogen concentration can now be predicted. Moreover, we have investigated the magnetic structures of the YCo_3 hydrides, especially the β_2 and γ phases, through NPD. In the magnetic structures, the exchange interaction is sensitive to the separation between the magnetic atoms, so the various Co-Co distances have been calculated to understand the magnetic properties of YCo_3 and its three hydrides.

In Part I of this paper, the results of *ab initio* calculation and NPD measurements on the crystal and magnetic structures of YCo_3 are presented and discussed.¹² The organization of Part II of the paper is as follows. Section II describes the experimental techniques. In Sec. III, we first discuss the structural refinement and then demonstrate that the D site occupancies determined are consistent with the Westlake model.^{10,11} We then describe the magnetic structure derived from the neutron diffraction data. Finally, in Sec. IV, we discuss how the changes in the magnetic structure with hydrogenation can be explained in terms of the changes in Co-Co distances between the different phases.

II. EXPERIMENTAL DETAILS

The polycrystalline alloy YCo_3 was prepared by arc melting Y (99.9% purity) and Co (99.9+ % purity) metal pieces in an argon atmosphere, followed by annealing at 1050 °C in an argon atmosphere for seven days. The hydride samples were prepared by the Sievert's volumetric method. The synchrotron x-ray-diffraction measurements were made at Station 9.1, at the SRS, U.K., using a capillary sample container. The *in situ* time-of-flight NPD experiments on YCo_3 deuterides were carried out at OSIRIS, ISIS, U.K., with a cryostat to go to low temperatures. Following increases in the *in situ* hydrogen pressure, the hydrogen was absorbed in the sample and the corresponding structure changed over a period of time during which the evolving diffraction patterns were recorded. The temperature range of the measurements was from 323 to 50 K, above and below the Curie or Néel temperatures. The crystal and magnetic structures of YCo_3 hydrides were then analyzed using GSAS,¹³ with the graphical user interface EXPGUI.¹⁴

III. RESULTS

A. Crystal structures

There are two serious problems in analyzing the structure of YCo_3 by x-ray-diffraction measurement using a normal laboratory $\text{Cu } K\alpha$ x-ray source. One problem is that $\text{Cu } K\alpha$ radiation is very close to the Co K absorption edge

(1.608 Å). Thus the x-ray fluorescence causes a very high background; the second problem is that the YCo_3 powder sample has strong preferred orientation. Thus monochromatic x rays (wavelength 1.0 Å), extracted from the SRS synchrotron source, were used to measure the diffraction pattern, except for the final sample ($x=4.5$), which was measured using a laboratory x-ray source ($\text{Cu } K\alpha$ x-ray source). On the SRS, the powder samples were mounted in a rotating capillary tube to remove most of the effects of preferred orientation.

The synchrotron radiation diffraction patterns for YCo_3 , $\text{YCo}_3\text{H}_{1.24}$, and $\text{YCo}_3\text{H}_{1.9}$, along with the laboratory source pattern for $x=4.5$, have been entered into GSAS and analyzed. The resulting lattice parameters, the atomic coordinates of Y and Co atoms, the unit cell volumes, and the relative expansions of YCo_3 and its three hydrides are shown in Table I. A_h is the powder absorption factor that has been applied to the synchrotron data. The absorption correction used is of the Debye-Scherrer form.¹³ The absorption factor correlates with the thermal coefficient U_{iso} , and therefore was not refined. The absorption correction would decrease the diffraction intensity mainly at low angles or large d spacing. If the absorption is not corrected for, it would lead to unrealistic values of the thermal coefficient, U_{iso} , particularly for strongly absorbing samples. For the case of the present YCo_3H_x samples, U_{iso} would go negative if it were not for the absorption correction. The XRD pattern for $\text{YCo}_3\text{H}_{4.5}$ was measured using a laboratory x-ray diffractometer (Siemens 5000), using Bragg-Brentano flat plate geometry; hence no absorption correction is needed. The anisotropic lattice expansion is observed again. For the β_1 and the β_2 phases, the lattice expands in the c direction, while a remains almost unaltered; going from the β_2 to the γ phase, the lattice expands in the a direction while c , surprisingly, shrinks by 0.25%. The unit cell volume is calculated for each phase. It is convenient to consider the volume expansion of the AB_2 and AB_5 units separately. For the β_1 and the β_2 phases, the volume of the AB_2 unit increases by 13.2% and 20.9%, respectively, but simultaneously the volume of the AB_5 unit decreases by 0.63% and 1.98%, respectively. The cell volume expansion is thus totally due to the expansion of the AB_2 unit. This is consistent with the conclusions of Benham *et al.*⁶ and suggests that the hydrogen atoms are entirely located at interstices in the AB_2 unit in both the β_1 and β_2 phases. For the γ phase, the volumes of both the AB_2 and AB_5 units increase. Thus hydrogen atoms must also fill sites in the AB_5 unit in this phase, allowing the a lattice parameter to increase. The volume expansion per hydrogen atom was also calculated for the three hydrides, being 3.08 Å³, 3.05 Å³, and 2.85 Å³, respectively. It thus takes decreasing volume expansion to accommodate each hydrogen atom as the hydrogen content increases. For the β_1 phase, most interstices are unoccupied although they are also expanded. For the β_2 and the γ hydrides, more interstices are occupied, thus the expansion is more uniform and so the volume expansion per hydrogen atom becomes smaller.

The position and hole sizes of the tetrahedral and octahedral interstices were calculated using the lattice parameters and atom coordinates given in Table I. The atomic radii of Y (1.80 Å) and Co atoms (1.35 Å) follow those used by Ben-

TABLE I. Lattice parameters, volume expansion, and atom positions for YCo₃H_x: space group *R-3m*, measured with synchrotron XRD. *V*: Volume of YCo₃ unit cell, $V=3V_1+3V_2$. *V*₁: Partial volume of YCo₂-type structure unit. *V*₂: Partial volume of YCo₅-type structure unit.

<i>x</i>	0	1.24	1.9	4.5 ^a
Phase	α	B ₁	B ₂	γ
<i>a</i> (Å)	5.0159(1)	5.0190(1)	5.0025(1)	5.2730(3)
<i>c</i> (Å)	24.3729(2)	25.9189(7)	26.9104(10)	26.8440(36)
Y ₁ (3 <i>a</i> ,0,0,0)				
Uiso (Å ²)	0.0318(11)	0.0138(13)	0.0049(8)	0.0411(70)
Y ₂ (6 <i>c</i> ,0,0, <i>z</i>)	0.1411(1)	0.1332(2)	0.1302(1)	0.1330(4)
Uiso (Å ²)	0.0285(7)	0.0137(10)	0.0025(10)	0.0324(50)
Co ₁ (3 <i>b</i> ,0,0,1/2)				
Uiso (Å ²)	0.0190(15)	0.0100(20)	0.0099(25)	0.0218(97)
Co ₂ (6 <i>c</i> ,0,0, <i>z</i>)	0.3337(1)	0.3333(2)	0.3335(3)	0.3331(6)
Uiso (Å ²)	0.0146(10)	0.0115(14)	0.0211(19)	0.0697(81)
Co ₃ (18 <i>h</i> , <i>x</i> ,− <i>x</i> , <i>z</i>)	0.5006(4)	0.4974(6)	0.4996(7)	0.4870(11)
	0.4994(4)	0.5026(6)	0.5004(7)	0.5130(11)
	0.0809(1)	0.0755(1)	0.0722(1)	0.0762(3)
Uiso (Å ²)	0.0125(6)	0.0040(7)	0.0011(8)	0.0123(33)
<i>A</i> _{<i>h</i>} = $\mu R/\lambda$	6.78	4.0	4.2	N/A
<i>R</i> <i>p</i> (−background)	0.0752	0.0728	0.0842	0.0164
<i>V</i> (Å ³)	531.05(2)	565.43(3)	583.21(3)	646.39(9)
$\Delta V/V$ (%)		6.5	9.8	21.7
$\Delta V/H$ atom (Å ³)		3.08	3.05	2.85
<i>V</i> ₁ (Å ³)	91.10(1)	103.10(1)	110.18(1)	116.95(2)
$\Delta V_1/V_1$ (%)		13.2	20.9	28.4
<i>V</i> ₂ (Å ³)	85.92(1)	85.38(1)	84.22(1)	98.51(1)
$\Delta V_2/V_2$ (%)		−0.63	−1.98	14.7

^aThe data of YCo₃H_{4.5} is from the refinement of the powder XRD pattern using a laboratory Cu *K* α x-ray source, the others are from synchrotron x-ray diffraction.

ham *et al.*,⁶ which were taken from the compilation by Slater.¹⁵ The resulting hole sizes are listed in Table II. We consider first the interstitial sites entirely within the *AB*₂ and *AB*₅ units and then the interstices, 18*h*₁ and 18*h*₂, that are situated at the boundary between the *AB*₂ and *AB*₅ units. The interstices in the *AB*₅ unit and at the boundary between the *AB*₂ and *AB*₅ units show no expansion in either the β_1 or the β_2 hydrides, while the interstices within the *AB*₂ unit show considerable expansion. This again suggests that, in the β_1 and β_2 phases, the hydrogen atoms are restricted to interstices in the *AB*₂ unit, consistent with the measured cell volume expansion. For the γ hydride, the interstices in the *AB*₅ unit also show considerable expansion, suggesting that, in this phase, sites in this block also contain hydrogen.

In order to fully refine the hydride (deuteride) structures, four neutron powder diffraction patterns were recorded *in situ* for YCo₃D_{*x*} single phase samples (*x*=0,1.3,2.0,4.6) above the respective magnetic ordering temperatures. The resulting patterns were entirely indexed according to the *R-3m* space group. The refinements of the crystal structures of YCo₃D_{*x*} were started using the lattice parameters and atom coordinates of Y and Co taken from the x-ray data, and various deuterium site occupancies were tried, starting from the bigger interstices, as listed in Table II. According to the

geometric model—which requires a hole size of at least 0.4 Å radius as suggested by Westlake^{10,11}—the interstices 6*c*₁, 18*h*₃, and 18*h*₇/36*i*₁ in the *AB*₂ unit are the most probable sites for deuterium atoms in the β_1 and the β_2 hydrides. In the γ hydride, the 18*h*₂ and 18*h*₁ interstices at the boundary between the *AB*₂ and *AB*₅ units, and the 18*h*₅, 6*c*₂, and 9*e*/36*i*₂ interstices in the *AB*₅ units are also enlarged sufficiently for deuterium occupancy.

The refined neutron diffraction patterns of the crystal structures of YCo₃D_{*x*} (*x*=0,1.3,2.0,4.6) are shown in Fig. 1. One point to note is that it is necessary to correct for the neutron absorption in cobalt, as otherwise, the thermal displacement parameters would go negative, in the same way as in the refinements of the x-ray diffraction patterns. The best Rietveld refinement placed the deuterium atoms at the 18*h*₇/36*i*₁ site for both the β_1 and the β_2 hydrides, giving site occupancies of 0.662 and 1.0 and *R**p* values of 0.0287 and 0.0385, respectively (see Table III). This conclusion is consistent with the results reported earlier by Benham *et al.*⁶ It should be noted that there are small differences in the refined lattice parameters between the x-ray and NPD refinements, which are consistent with the small differences in the measured H content. As the H concentrations employed all lie in one-phase regions, these small changes are as expected.

TABLE II. Interstitial holes sizes for YCo_3H_x calculated using atomic radii: $r_{\text{Y}}=1.78$, and $r_{\text{Co}}=1.25$ (Å).

	Site	Type	$r(x=0)$	$r(x=1.24)$	$r(x=1.9)$	$r(x=4.5)$
YCo ₂ layer	6c ₁	YCo ₃	0.32	0.50	0.60	0.63
	6c ₃	Co ₄	0.30	0.36	0.43	0.37
	18h ₃	Y ₂ Co ₂	0.28	0.45	0.54	0.56
	18h ₆	YCo ₃	0.29	0.34	0.40	0.39
	18h ₇ ^a	Y ₃ Co ₂	0.22	0.38	0.48	0.45
	36i ₁ ^a	Y ₂ Co ₂	0.28	0.41	0.49	0.49
YCo ₂ -YCo ₅ layer boundary	18h ₁	Y ₂ Co ₂	0.34	0.33	0.34	0.40
	18h ₂	Y ₂ Co ₂	0.33	0.34	0.34	0.45
YCo ₅ layer	6c ₂	Co ₄	0.27	0.28	0.26	0.43
	6c ₄	Co ₄	0.27	0.25	0.26	0.26
	9e ^b	Y ₂ Co ₄	0.20	0.20	0.19	0.27
	36i ₂ ^b	YCo ₃	0.33	0.33	0.32	0.41
	18h ₄	YCo ₃	0.32	0.31	0.31	0.37
	18h ₅	YCo ₃	0.32	0.32	0.31	0.44

^aThe names and types of the interstitial sites follow Ref. 6 except 18h₇, which is added by us. An 18h₇ site is surrounded by two tetrahedral 36i₁ sites. The five atoms (Y₃Co₂) coordinating the 18h₇ site are the same five atoms that constitute the two 36i₁ sites.

^bAn octahedral 9e site is surrounded by four 36i₂ tetrahedral sites. The six atoms (Y₂Co₄) coordinating the 9e site are the same six atoms that constitute the four 36i₂ sites. This is not mentioned in Ref. 6.

There may also be small increases in the hydride lattice parameter relative to the deuteride due to the greater zero point energies but these have not been quantified in this work.

Turning to the γ phase, Fourier difference maps of the basal planes at different heights in $\text{YCo}_3\text{D}_{4.6}$ (Fig. 2) suggest that deuterium atoms occupy the 18h₇/36i₁ sites but also the 9e/36i₂, 18h₂, and 18h₁ sites. The best Rietveld fit for multiple site occupation shows that all the above sites, except 18h₁, are occupied by deuterium. The lattice parameters, the atom coordinates of the metal atoms, and the deuterium site occupancies are listed in Table III. The R_p value for this fit is 0.0245. The coordinates of deuterium at the 18h₇/36i₁ site are given as for the 18h site, and those at 9e/36i₂ are given as for the 36i site. The crystal structure of $\text{YCo}_3\text{D}_{4.6}$, including the deuterium sites, is shown in Fig. 3. For $x=4.6$, the occupation probabilities for the 18h₇/36i₁, 18h₂, and 36i₂/9e sites are 1.0, 1.0, and 0.162, respectively.

B. Rationalization of H sites using the Westlake model

The deuterium site occupancies as determined are consistent with previous investigations of YCo_3D_x . Benham *et al.* found that only the 18h₇/36i₁ site in the AB_2 unit is filled for $\text{YCo}_3\text{D}_{1.0}$ and $\text{YCo}_3\text{D}_{1.9}$,⁶ although at that time the β_1 and the β_2 were thought to be a single β phase. Bartashevich *et al.*⁸ showed that deuterium occupies the same three types of sites for the γ phase, $\text{YCo}_3\text{D}_{3.8}$, but at a lower deuterium content and with different site occupancies than observed here. It is interesting to see whether these occupancies can be understood in terms of the geometric model developed by Westlake,^{10,11} which requires that H(D) occupies interstitial sites of radius at least 0.4 Å radius with an H-H (D-D) separation

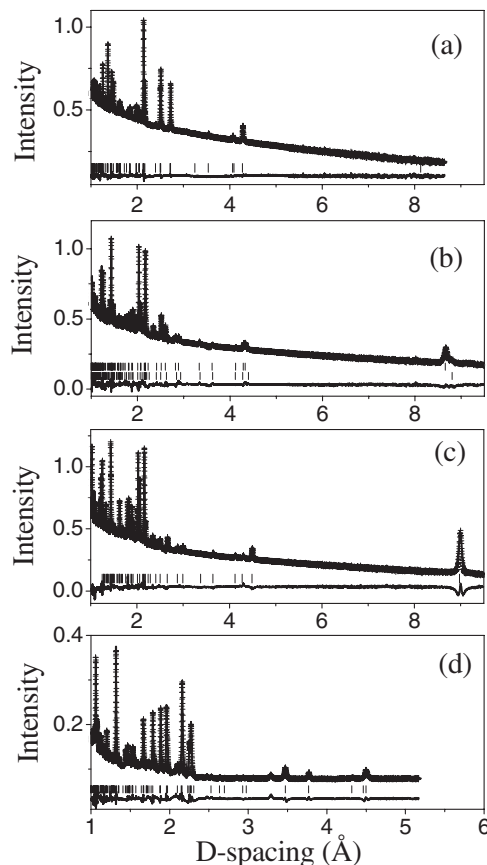


FIG. 1. Refined neutron powder diffraction patterns of YCo_3D_x : (a) $x=0$, in V can, 291 K; (b) $x=1.3$, in Al can, 290 K; (c) $x=2.0$ in Al can, 250 K; and (d) $x=4.6$, in V can, 156 K.

TABLE III. The lattice parameters, atom coordinates of the metal atoms, and deuterium site occupancy derived from the refined neutron powder diffraction patterns of YCo_3D_x .

x	0	1.3	2.0	4.6
Phase	α	β_1	β_2	γ
a (Å)	5.0152(1)	5.0209(1)	4.9992	5.2666(1)
c (Å)	24.3805(8)	25.9569(18)	26.9295	26.7753(8)
Y_1 ($3a, 0, 0, 0$)				
Uiso (Å ²)	0.0060(9)	0.0090(13)	0.0091	0.0156(14)
Y_2 ($6c, 0, 0, z$)	0.1423(1)	0.1299(1)	0.1298	0.1330(1)
Uiso (Å ²)	0.0051(6)	0.0140(10)	0.010	0.0071(12)
Co_1 ($3b, 0, 0, 1/2$)				
Uiso (Å ²)	0.0101(10)	0.0270(32)	0.012	0.0007(10)
Co_2 ($6c, 0, 0, z$)	0.3340(2)	0.3340(3)	0.3341	0.3354(4)
Uiso (Å ²)	0.0120(16)	0.0068(23)	0.013	0.0104(30)
Co_3 ($18h, x, -x, z$)	0.4992(5)	0.4930(10)	0.5032	0.4870(12)
	0.5008(5)	0.5070(10)	0.4968	0.5130(12)
	0.0816(2)	0.0716(2)	0.0713	0.0762(3)
Uiso (Å ²)	0.0061(9)	0.0190(14)	0.008	0.0093(10)
D_1 ($18h_7, x, -x, z$)/(36 i_1)		0.5101(6)	0.5021	0.4989(4)
		0.4899(6)	0.4979	0.5011(4)
		0.1359(1)	0.1351	0.1375(1)
occupancy		0.662	1.0	1.0
Uiso (Å ²)		0.0530(8)	0.012	0.0234(6)
D_2 ($18h_2$)				0.8478(4)
				0.1522(4)
				0.0677(1)
occupancy				1.0
Uiso (Å ²)				0.0126(5)
D_3 ($36i_2, x, y, z$)/(9 e)				0.5104(19)
				0.5046(40)
				0.00684(40)
occupancy				0.162
Uiso (Å ²)				0.0088(9)
R_p (–background)	0.0180	0.0287	0.0385	0.0245

^aThe occupancies of the metal atoms are all 1.TABLE IV. Nearest-neighbor interstitial sites separations for $\text{YCo}_3\text{H}_{1.3}$.

Sites separations (Å)		YCo_2 layer						
		$6c_1$	$6c_3$	$18h_3$	$18h_6$	$18h_7$	$36i_1$	
YCo_2 layer	$6c_1$	4.05	2.90	0.73	2.58	1.60	1.63	
	$6c_3$	2.90	3.22	2.64	0.87	1.69	1.72	
	$18h_3$		0.73	2.64	1.22	2.13	1.36	1.25
					2.90		2.22	
	$18h_6$	2.58	0.87	2.13	1.45	1.41	1.27	
	$18h_7$		1.60	1.69	1.36	1.41	2.06	0.32
				2.22		2.51		
	$36i_1$	1.63	1.72	1.25	1.27	0.32	0.64	

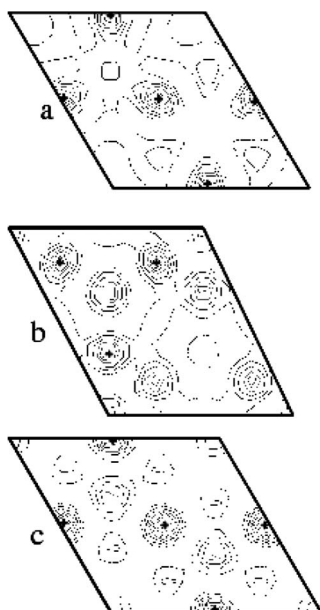


FIG. 2. Fourier difference maps of the basal planes of $\text{YCo}_3\text{D}_{4.6}$: (a) $z=0.139$, $18h_7/36i_1$ site; (b) $z=0.067$, $18h_2$ site; and (c) $z=0$, $9e/36i_2$ site. The relevant site is marked by “+.”

ration of at least 2.1 Å. Hydrogen site occupancies in AB_5 and in AB_2 (both hexagonal and cubic Laves phase) compounds have both been successfully rationalized using this model.¹⁶

Having already demonstrated that the site radii are consistent with the Westlake model, we will now consider how the second criteria, the minimum H-H distance influences the deuterium site occupancies in YCo_3D_x . The nearest-neighbor D-D site separations for YCo_3D_x ($x=1.3, 1.9$, and 4.5) are tabulated in Tables IV–VI. For $\text{YCo}_3\text{D}_{1.3}$, the sites $6c_1$, $18h_3$, and $36i_1$ are larger than 0.4 Å, and the preferred occupancy should be in the above order. The $6c_1$ site is considered first. The shortest $6c_1$ - $6c_1$ distance is 4.05 Å. Thus all $6c_1$ sites can be filled. The $18h_7$ (hole size 0.38 Å) should also be considered in this context because the five atoms (three Y and two Co atoms) coordinating this site are the same five atoms that constitute the two $36i_1$ sites. The nearest $6c_1$ - $18h_3$, $6c_1$ - $18h_7$, and $6c_1$ - $36i_1$ distances are 0.73, 1.60,

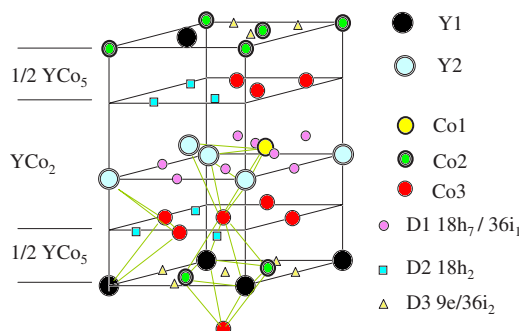


FIG. 3. (Color online) Crystal structures of $\text{YCo}_3\text{D}_{4.6}$.

and 1.63 Å. Thus one filled $6c_1$ site would block three $18h_3$, three $18h_7$, and six $36i_1$ sites. If all the $6c_1$ sites are filled, all the $18h_3$, $18h_7$, and $36i_1$ sites would be blocked; thus the hydride would be $\text{YCo}_3\text{D}_{0.67}$, which is a deuterium content lower than the observed minimum hydrogen content of $x=1.2$ for the β_1 hydride. Hence the $18h_3$ site must be considered to be filled first. One of every three $18h_3$ sites can be filled, and six $18h_7$ sites can then be filled while satisfying the minimum D-D distance. The formula of deuteride occupancy is consistent with the observed deuterium content. Now we consider filling the $18h_7/36i_1$ site first. The nearest $18h_7$ - $18h_7$ distances are 2.06 and 2.51 Å. There are nine $18h_7/36i_1$ sites around one Y_1 atom, and six of them can be filled without violating the 2.1 Å least H-H distance. Considering the packing of the polyhedra, fewer deuterium atoms can actually be accommodated; but the shortest $18h_7$ - $18h_7$ distance, 2.06 Å, is very close to 2.1 Å, and so this site separation would be enough if deuterium atoms are displaced from the center of the site. We thus suppose that 2/3 of the $18h_7/36i_1$ sites can still be filled, and all the $6c_1$ and $18h_3$ sites would be blocked. Thus the deuteride would also be $\text{YCo}_3\text{D}_{1.33}$. Hence we have two models of deuterium occupancy that are both consistent with the deuterium content of $\text{YCo}_3\text{D}_{1.3}$. Rietveld fitting of the $\text{YCo}_3\text{D}_{1.3}$ neutron diffraction pattern, in fact, supports the latter case. From the atom coordinates of neutron diffraction results listed in Table III, the calculated $18h_7$ - $18h_7$ distance is 2.22 Å. This increase relative to the separation of the sites is because the deuterium

TABLE V. Nearest-neighbor interstitial site separations for $\text{YCo}_3\text{H}_{1.9}$.

Sites separations (Å)		YCo ₂ layer					
		$6c_1$	$6c_3$	$18h_3$	$18h_6$	$18h_7$	$36i_1$
YCo ₂ layer	$6c_1$	4.02	2.90	0.60	2.59	1.48	1.50
	$6c_3$	2.90	3.36	2.68	0.79	1.75	1.77
	$18h_3$	0.60	2.68	1.01	2.23	1.27	1.19
				3.06		2.00	
	$18h_6$	2.59	0.79	2.23	1.33	1.47	1.38
					3.02	2.38	
	$18h_7$	1.48	1.75	1.27	1.47	2.24	0.24
				2.00	2.38	2.37	
	$36i_1$	1.50	1.77	1.19	1.38	0.24	0.48

TABLE VI. Nearest-neighbor interstitial sites separations for $\text{YCo}_3\text{H}_{4.5}$.

Sites separations (\AA)	YCo_2 layer						$\text{YCo}_2\text{-YCo}_5$ boundary		YCo_5 layer						
	$6c_1$	$6c_3$	$18h_3$	$18h_6$	$18h_7$	$36i_1$	$18h_1$	$18h_2$	$6c_2$	$6c_4$	$9e$	$36i_2$	$18h_4$	$18h_5$	
YCo_2 layer	$6c_1$	4.29	3.05	0.77	2.71	1.70	1.74	2.90	2.08	1.28	3.38	3.33	2.97	3.25	2.12
	$6c_3$	3.05	3.25	2.77	0.97	1.77	1.81	2.08	2.85	3.26	1.35	3.23	2.88	2.12	3.12
	$18h_3$	0.77	2.77	1.29	2.22	1.43	1.31	2.43	1.68	1.66	3.21	3.43	2.94	2.96	2.00
				3.05		2.33									
	$18h_6$	2.71	0.97	2.22	1.60	1.47	1.30	1.59	2.29	3.06	1.87	3.39	2.88	2.05	2.77
					2.86	2.53									
$\text{YCo}_2\text{-YCo}_5$ Layer boundary	$18h_7$	1.70	1.77	1.43	1.47	2.13	0.38	2.57	2.54	2.55	2.71	3.74	3.32	2.99	2.88
				2.33	2.62										
	$36i_1$	1.74	1.81	1.31	1.30	0.38	0.75	2.36	2.34	2.58	2.73	3.76	3.28	2.88	2.77
	$18h_1$	2.90	2.08	2.43	1.59	2.57	2.36	2.17	1.29	2.65	1.82	2.45	1.81	0.92	1.74
									2.58			2.52			
	$18h_2$	2.08	2.85	1.68	2.29	2.54	2.34	1.29	2.31	1.71	2.66	2.41	1.78	1.80	0.78
YCo_5 layer							2.58				2.47	2.47	2.58		
	$6c_2$	1.28	3.26	1.66	3.06	2.55	2.58	2.65	1.71	4.54	3.05	2.27	2.02	2.72	1.27
	$6c_4$	3.38	1.35	3.21	1.87	2.71	2.73	1.82	2.66	3.05	4.28	2.14	1.91	1.26	2.68
	$9e$	3.33	3.23	3.43	3.39	3.74	3.76	2.45	2.41	2.27	2.14	2.64	0.67	1.77	1.84
	$36i_2$	2.97	2.88	2.94	2.88	3.32	3.28	1.81	1.78	2.02	1.91	0.67	0.92	1.25	1.31
								2.52	2.47			0.99	1.35		
	$18h_4$	3.25	2.12	2.96	2.05	2.99	2.88	0.92	1.80	2.72	1.26	1.77	1.25	2.06	1.86
	$18h_5$	2.12	3.12	2.00	2.77	2.88	2.77	1.74	0.78	1.27	2.68	1.84	1.31	1.86	2.05

atoms are displaced from the centers of the site. Turning to the β_2 phase, it may be noted that all the interstitial holes in the YCo_2 layer of $\text{YCo}_3\text{D}_{1.9}$ are big enough to accommodate hydrogen atoms. Thus the criterion for the D-D distance becomes very important. According to the hole sizes, the preferred occupancy would be in the sequence $6c_1$, $18h_3$, $18h_7/36i_1$, $6c_3$, and $18h_6$. If the $6c_1$, $18h_3$, $6c_3$, or $18h_6$ sites are filled first, the total number of hydrogen atoms per unit cell is 12, and the formula is thus $\text{YCo}_3\text{H}_{1.33}$, which is not consistent with the hydrogen content of this hydride. However, if the $18h_7/36i_1$ site is filled first, all these sites can be filled because the nearest $18h_7$ - $18h_7$ separation is 2.24 \AA . Alternatively, one in each pair of $36i_1$ sites is filled. All the other interstitial sites are now blocked. Thus the total number of hydrogen atoms in a unit cell is 18, and the formula is YCo_3H_2 , which is consistent with the hydrogen content of $\text{YCo}_3\text{H}_{1.9}$. Hence, we can conclude that the filling of the $18h_7/36i_1$ sites is the only possible choice and this is again supported by the fitting of the neutron diffraction pattern of YCo_3D_2 .

Thus the same interstitial sites, $18h_7/36i_1$, are occupied in both the β_1 and β_2 hydrides with site occupancies of $2/3$ and 1, respectively, the restricted occupancy being due to the constraints caused by the smaller lattice parameter in the β_1 phase. This is consistent with the fact that there is a critical point at 120 $^\circ\text{C}$, above which only one phase is seen.⁹ The phase diagram must therefore resemble the α - β phase separation in Pd/H, in that the concentration of H can be varied

continuously at temperatures above a critical point in a single phase region.¹⁷ We should note that, at these higher temperatures, the magnetic properties should vary continuously with D content.

In $\text{YCo}_3\text{H}_{4.5}$, the interstitial holes at the $\text{YCo}_2\text{-YCo}_5$ layer boundary and in the YCo_5 layer are both enlarged enough to accommodate deuterium atoms. It is still convenient to consider the YCo_2 and the YCo_5 layers separately. The preferred occupancy in the YCo_2 layer should be in the sequence $6c_1$, $18h_3$, $18h_7/36i_1$, and $18h_6$ according to the hole sizes, while the $6c_3$ hole is not big enough to be filled, contrary to the case of $\text{YCo}_3\text{H}_{1.9}$. Hydrogen site occupancy is similar to that in $\text{YCo}_3\text{H}_{1.9}$. Only the $18h_7/36i_1$ sites can be filled, and all the other holes in the YCo_2 layer are then blocked. The preferred occupancy of the holes at the boundary of the $\text{YCo}_2\text{-YCo}_5$ layers and in the YCo_5 layer should be in the order $18h_2$, $18h_5$, $6c_2$, $9e/36i_2$, and $18h_1$ according to the hole size criterion. All eighteen $18h_2$ sites can be filled, and one in every four $36i_2$ sites or the central nine $9e$ sites can be filled. The total number of hydrogen atoms filled in a unit cell is thus 45, giving the formula YCo_3H_5 . We conclude that this is the maximum hydrogen concentration, because no more sites can be filled according to the geometric model. The site occupancy is supported by the fitting of the neutron diffraction pattern for $\text{YCo}_3\text{D}_{4.6}$. The deuterium site occupancies in the β_1 , β_2 , and γ phases thus comply with the Westlake criteria.

It should be noted that Filinchuk and Yvon¹⁸ have pointed out that these structures can also be rationalized in terms of

the coordination of the transition metal atom by the hydrogen atoms. Thus, in the Ni equivalent structures, such as γ -ErNi₃D_{3.7}, the Ni atom is tetrahedrally coordinated by D, whereas, in the equivalent Co structures (ErCo₃D_{4.6} and the present YCo₃D_{4.6}, the Co is surrounded by 4–6 D atoms in disordered, distorted octahedral configurations. On this view, the particular TM atom first dictates its local D site coordination but then the atoms adjust their positions such that the Westlake criteria are also satisfied.

C. Magnetic structures

NPD is the primary technique used for determining magnetic structures. However, in the YCo₃D_x system, the Y and D atoms have much larger coherent neutron scattering cross sections [Y: 7.55, D: 5.59, and Co: 0.779 b (Ref. 19)] than the magnetic scattering from the Co atoms. Thus, in the neutron diffraction spectra of this system, the nonmagnetic Y atom and D atoms make a much more significant contribution to the diffraction pattern than does a magnetic Co atom. The contribution from the D atoms also becomes more significant with increasing D content making it quite difficult to extract the magnetic structure. However, given the good resolution and intensity of the OSIRIS instrument, the magnetic structure has been determined with good accuracy.

Since the β_1 hydride phase is paramagnetic, we focused our studies of magnetic structures on the β_2 and γ phases. The YCo₃D₂ NPD pattern (Fig. 4), measured with no field at 50 K (i.e., below the Curie point), has been analyzed, with its crystal structure assumed to be space group $R\bar{3}m$ and its magnetic structure to be magnetic space group $*R\bar{3}m'$. The directions of the magnetic moments of all three types of Co atoms are found to be close to the “z” direction. The diffraction pattern was taken using an Al sample can, so six Al peaks are seen, marked as ticks in Fig. 4. YCo₃D₂ is found to have a ferromagnetic structure. The refinements of the diffraction patterns with and without magnetic diffraction are shown in Fig. 4. The inset plot shows the refinement of the diffraction peak (10 $\bar{2}$) ($d=4.1134$ Å). It can be clearly seen that the quality of refinement is much better with magnetic diffraction included. The magnetic unit cell is the same as the nuclear unit cell, there being no superlattice peaks. The magnetic moments of Co atoms are shown in Table VII. The average magnetic moment is $0.767(51)\mu_B/\text{Co}$.

The YCo₃D_{4.8} NPD pattern, taken in the Al tube at 100 K, has also been analyzed using GSAS. In GSAS, the magnetic symmetry is described with a crystal space group and a spin-flip model. There are three unique symmetry operators for $R\bar{3}m$: M100, 2100, and a rhombohedral center of symmetry. We find the structure of YCo₃D_{4.8} to be antiferromagnetic (see below). Therefore, in the absence of a superlattice, in this phase, Co₁ has to be paramagnetic because of its site symmetry. Co₂ has magnetic moments only along the z direction in an antiferromagnetic arrangement. Co₃ can have magnetic moments along all three directions in an antiferromagnetic arrangement, but in fact, its magnetic moment is mainly along the z direction.

Figure 5 shows the refined diffraction pattern of YCo₃D_{4.8} in an antiferromagnetic arrangement, as well as the observed

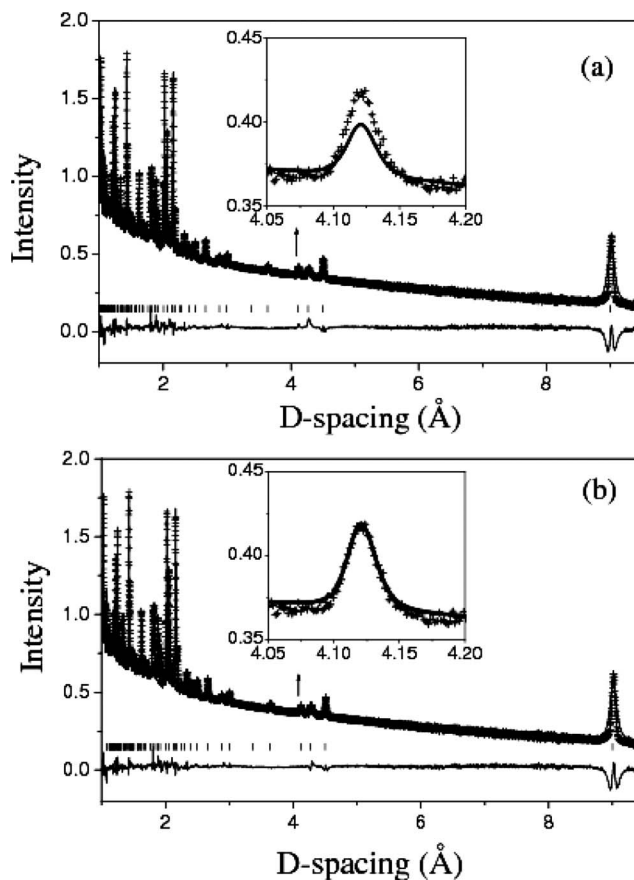


FIG. 4. Refinement of YCo₃D₂ neutron powder diffraction pattern at 50 K: (a) crystal structure only, and (b) crystal and ferromagnetic structure.

data and the difference between the calculated and the observed patterns. There are three lines of markers showing the diffraction peaks for the three phases. The first line shows the peak positions for YCo₃D_{4.8} nuclear diffraction, the second line shows diffraction peaks from the Al tube, and the third line shows peaks for the YCo₃D_{4.8} magnetic diffraction only. For YCo₃D_{4.8}, the peak positions for nuclear and magnetic diffraction are entirely coincident. Thus there are no superlattice peaks, and the magnetic unit cell is the same as for the nuclear unit cell. The magnetic moments of the Co atoms are

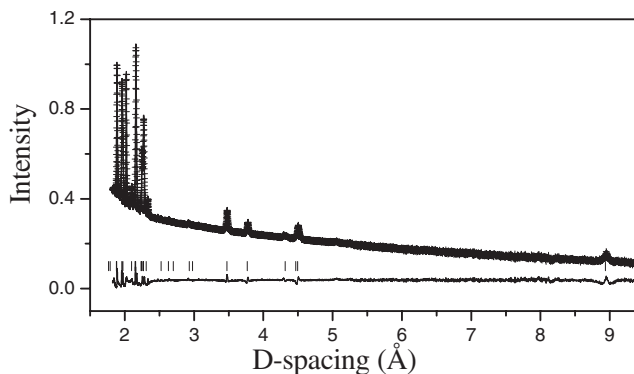


FIG. 5. Refinement of YCo₃D_{4.8} neutron powder diffraction pattern at 100 K in an antiferromagnetic structure.

TABLE VII. The magnetic moments of YCo_3D_2 and $\text{YCo}_3\text{D}_{4.8}$ from the refinements of the NPD pattern.

	Co_1 (μ_B)	Co_2 (μ_B)	Co_3 (μ_B)	Average moment (μ_B/Co)	χ^2	wR_p (-background)	R_p (-background)
YCo_3D_2 ferromagnetic	0.026 (77)	0.485 (70)	0.984 (41)	0.767 (51)	37.18	0.0281	0.0507
$\text{YCo}_3\text{D}_{4.8}$ antiferromagnetic	0	1.20 (27)	-0.15 (20)		39.88	0.0282	0.0268

listed in Table VII. The magnetic moments of Co_2 and Co_3 are $1.20(27)\mu_B/\text{Co}$ and $-0.15(20)\mu_B/\text{Co}$, respectively.

IV. DISCUSSION

Having established and rationalized the D positions and their influence on the D-concentration dependence of the two lattice parameters and having determined the measured magnetic structures in terms of the various magnetic moments on the Co atoms, we are now in a position to establish a rationalization of the dramatic changes seen in the magnetic properties of this system as a function of H(D) concentration. The evidence from both Part I and the present work strongly supports the argument that the main driving force is the cobalt-cobalt distance, as originally pointed out by Néel.^{20,21} A similar correlation, plotting the exchange interaction against the ratio d/r_d is known as the Bethe-Slater curve.²² Thus Néel concluded that the coupling varies as a function of $(d-2r)$ where d is the interatomic spacing and r is the radius of the d band (~ 0.72 Å) giving a $(d-2r)$ value for the critical spacing of around 1 Å and hence a critical value of the Co-Co distance of around 2.44 Å. Below this separation, the coupling is antiferromagnetic and above it, it is ferromagnetic. However, we might expect this crossover point to be influenced to some extent by changes in the band structure and so it may shift somewhat between phases. Finally, beyond the ferromagnetic coupling range, we might expect there to be a further weak antiferromagnetic coupling region, due to Friedel oscillations of the spin density. The various shortest Co-Co distances are given in Table VIII, where the values for the YCo_3 metallic lattice are taken from the crystal structure as reported in Part I. It should be noted that all the minimum

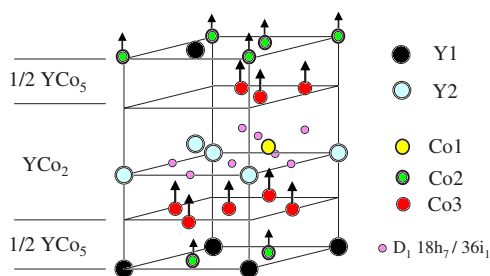
$\text{Co}_1\text{-Co}_1$, $\text{Co}_2\text{-Co}_2$, and $\text{Co}_3\text{-Co}_3$ distances are all in the basal plane.

If we first apply these arguments to the metallic phase, we see that the Co_2 and Co_3 layers are both ferromagnetically coupled within the layers. We next note that the $\text{Co}_1\text{-Co}_3$ distance is also clearly ferromagnetic. Hence, the Co_1 and Co_3 layers are both clearly coupled together ferromagnetically. However, both the $\text{Co}_2\text{-Co}_3$ separations are on the antiferromagnetic side of the crossover and hence the Co_3 layers either side of the Co_2 layers should be antiferromagnetically coupled. Thus the overall structure is ferrimagnetic as concluded in Part I. However, we would also note from the spin-density calculations and the high field magnetization measurements reported there that the spin of the Co_2 can be flipped into a parallel orientation by a relatively small magnetic field. Hence we can conclude that the crossover separation in this phase must be close to 2.445 Å.

Now let us consider the effects of adding D to the structure to form the β_1 phase. This causes the c dimension to increase, the change being associated with the YCo_2 layer so that the corresponding $\text{Co}_2\text{-Co}_3$ distance increases into the ferromagnetic regime. The other main change is that the longer $\text{Co}_3\text{-Co}_3$ distance increases while the shorter decreases, getting close to the transition point. Moreover, as the $36i_1$ sites are only partially occupied, and there is a corresponding increase in the isotropic U value for the Co_3 atoms, we can reasonably expect that some or all of the short $\text{Co}_3\text{-Co}_3$ distances correspond to antiferromagnetic coupling. However, antiferromagnetic coupling on a triangular arrangement gives a “frustrated” structure so that the Co_3 layer would become paramagnetic. Thus, as the primary coupling

TABLE VIII. Co-Co separations in YCo_3H_x .

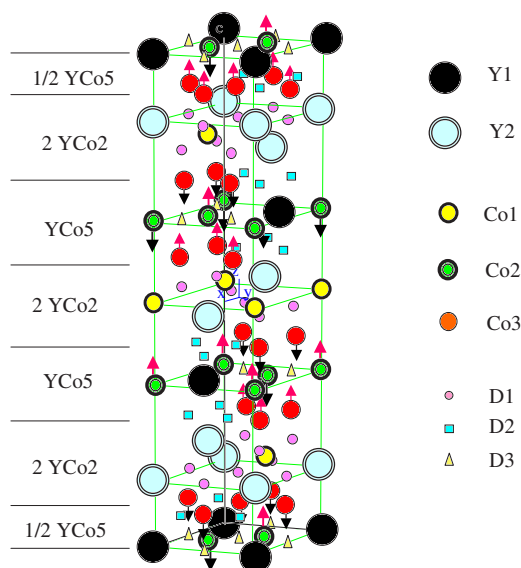
	$\text{Co}_1\text{-Co}_1$ (Å)	$\text{Co}_2\text{-Co}_2$ (Å)	$\text{Co}_3\text{-Co}_3$ (Å)	$\text{Co}_1\text{-Co}_3$ (Å)	$\text{Co}_2\text{-Co}_3$ (Å)
YCo_3	5.0159(1)	2.8960(1)	2.499(6) 2.517(6)	2.5468(26)	2.4414(25) 2.4496(27)
$\text{YCo}_3\text{H}_{1.24}$, β_1	5.0190(1)	2.8978(1)	2.4708(1) 2.5482(1)	2.7600(1)	2.4219(1) 2.4483(1)
$\text{YCo}_3\text{H}_{1.9}$, β_2	5.0025(1)	2.8882(1)	2.4952(1) 2.5073(1)	2.870(1)	2.4141(1) 2.4257(1)
$\text{YCo}_3\text{H}_{4.8}$, γ	5.2666(1)	3.040(10)	2.420(14) 2.843(14)	2.810(14)	2.428(8) 2.646(7)

FIG. 6. (Color online) YCo_3D_2 magnetic structure.

of the Co_1 and Co_2 atoms are to the Co_3 atoms it is not surprising that this phase is paramagnetic.

The magnetic structure of the β_2 hydride YCo_3D_2 is shown in Fig. 6. Here, experimentally, the Co_1 atom has a very small magnetic moment, $0.026(77)\mu_B$, and its value is well below the error in its determination. Thus we suppose that the Co_1 atom is actually paramagnetic or possibly weakly ferrimagnetically coupled, as suggested by the *ab initio* spin-density calculations.² It should be noted that the average magnetic moment/Co atom in the β_2 hydride is actually larger than in YCo_3 itself,^{1,3,9} a result that is quite abnormal in magnetic metal hydrides. This is because the antiparallel spin on the Co_1 atom in the metallic phase has been reduced. Let us now consider the Co-Co separations in this phase. Here, the Co_3 - Co_3 distance has increased to 2.49/2.50 Å. Moreover, all the $36i_1$ sites are now full and the isotropic U value has shrunk to its normal value. It is therefore reasonable to conclude that the Co_3 layers have become firmly ferromagnetic again. However, the Co_2 - Co_3 distances have shrunk to 2.41/2.42 Å, which would suggest antiferromagnetic coupling between the Co_2 and the Co_3 layers while we know that these layers are clearly ferromagnetically coupled. Here, we can only assume that band filling has reduced the crossover distance or that other Co-Co couplings along the c axis must predominate. Finally, we would note that the Co_1 - Co_3 distance is now 2.87 Å, which could be close to a second region of antiferromagnetic coupling (Friedel oscillation), which would account for the low and possibly ferromagnetic coupling of the Co_1 atom.

Now let us consider the γ phase, where we note that the a parameter has increased significantly while c has shrunk slightly. The other notable changes are that the short Co_3 - Co_3 distances are shorter (2.42 Å) while the long Co_3 - Co_3 distances are longer (2.84 Å) and the difference between the shorter Co_2 - Co_3 (2.43 Å) and the longer Co_2 - Co_3 (2.64 Å) has also increased. Experimentally, the Co_3 layers are internally ferromagnetic. We would note that the long Co_3 - Co_3 distance is ferromagnetic while the shorter distances are apparently antiferromagnetic. However, the shorter distances come in pairs while the longer distances form a continuous lattice and each Co_3 will experience two ferromagnetic interactions and one antiferromagnetic interaction so that overall ferromagnetism within the Co_3 layers is to be expected. Now, let us consider the coupling of the Co_2 layers above and below a Co_3 layer. The Co_2 layer lies between two Co_3 layers in such a way that alternate Co_2 atoms lie closer to the Co_3 in one layer than to the Co_3 in the other (the long and short distances in Table VIII). The corresponding separations are

FIG. 7. (Color online) $\text{YCo}_3\text{D}_{4.8}$ antiferromagnetic structure: Co_1 , paramagnetic; Co_2 and Co_3 , antiferromagnetic.

2.42 Å and 2.64 Å, respectively. If we assume that the former is antiferromagnetic and the latter is ferromagnetic, we see that the spin directions of the Co_2 atoms will alternate, making this layer internally antiferromagnetic while ensuring that the coupling between the two adjacent Co_3 layers, mediated by the intervening Co_2 atoms, will always be antiferromagnetic. Given that the Co_1 layer has zero spin in this phase, our proposed antiferromagnetic structure implies that the coupling between the Co_3 layer below a Co_1 layer to the next Co_3 above the Co_1 layer has to be ferromagnetic as all unit cells have the same spin orientations (Fig. 7). We must assume that this is due to some weaker long range interaction that stabilizes the same arrangement in successive unit cells. It is notable that it is only in the γ phase that the two Co_2 - Co_3 separations have split sufficiently for one to be antiferromagnetic and the other to be ferromagnetic. This might suggest that the reason for the Co_2 - Co_3 distances split so remarkably in the γ phase is that this allows the interactions to become clearly either ferromagnetic or antiferromagnetic. This would also suggest a band structure effect reminiscent of the displacive ordering (Peierls distortion) that is believed to drive the conductor-nonconductor transition in the YH_{2+x} system.²³

We can thus say that the remarkable changes in the magnetic structure of these systems as hydrogen is added can, in general, be explained as being due to the consequent changes in the Co-Co distances.

V. CONCLUSIONS

To avoid the high background caused by x-ray fluorescence and the effect of preferred orientation, an XRD experiment for YCo_3 has been carried out using synchrotron radiation, and more accurate lattice parameters and coordinates of Y and Co atoms have been determined. Neutron powder diffraction patterns of YCo_3D_x have been analyzed to determine deuterium site occupancies: the $18h_7/36i_1$ site for the β_1 and

β_2 hydrides, and the $18h_7/36i_1$, $18h_2$, and $9e/36i_2$ sites for the γ phase $\text{YCo}_3\text{D}_{4.6}$. The site occupancies were also successfully rationalized using the Westlake geometric model. The stoichiometric compositions of the β_1 and β_2 hydrides are $\text{YCo}_3\text{H}_{1.33}$ and YCo_3H_2 , respectively. We conclude that the saturated hydrogen content in the γ phase would be YCo_3H_5 .

Using magnetic neutron diffraction, we conclude that in the β_2 hydride $\text{YCo}_3\text{H(D)}_2$ the magnetic moments of the Co_2 and Co_3 atoms are all parallel with the Co_1 atom being paramagnetic while a rather complicated antiferromagnetic structure has been determined for the γ hydride $\text{YCo}_3\text{D}_{4.8}$. The Co-Co distances have been calculated for YCo_3 and its three hydrides. The magnetic structures can be largely rationalized on the assumption that adjacent spins are coupled antiferro-

magnetically if the Co-Co distance is less than about 2.44 Å and ferromagnetically for separations between about 2.44 and 2.84 Å. The notable displacement of the Co_3 atoms in the γ phase allows the interactions with the Co_2 atoms to split into clearly ferromagnetic and antiferromagnetic categories, which allows the system to adopt this complex antiferromagnetic structure. This transition is rather reminiscent of the displacive symmetry breaking transition in the YH_{2+x} structure that is believed to drive the analogous conducting-nonconducting transition in that system. We thus conclude that while much of the effect of H content on the magnetic structure of this system is driven by changes in the Co-Co distance, due to lattice expansion caused by the specific H site occupation, there are associated changes in the band structure.

-
- ¹M. Yamaguchi, H. Ikeda, T. Ohta, T. Katayama, and T. Goto, *J. Less-Common Met.* **106**, 165 (1985).
- ²X. Y. Cui, J. Liu, I. Morrison, and D. K. Ross, *J. Alloys Compd.* **404-406**, 136 (2005).
- ³M. Yamaguchi, D. K. Ross, T. Goto, and T. Ohta, *Z. Phys. Chem., Neue Folge* **145**, 355 (1985).
- ⁴M. Yamaguchi, I. Yamamoto, Y. Fugita, and T. Goto, *Z. Phys. Chem., Neue Folge* **163**, 677 (1989).
- ⁵M. I. Bartashevich, H. A. Katori, T. Goto, I. Yamamoto, and M. Yamaguchi, *Physica B* **201**, 135 (1994).
- ⁶M. J. Benham, S. M. Bennington, D. K. Ross, D. Noreus, and M. Yamaguchi, *Z. Phys. Chem., Neue Folge* **163**, 283 (1989).
- ⁷V. V. Burnasheva, V. A. Yartys, S. P. Solov'ev, N. V. Fadeeva, and K. N. Semenenko, *Sov. Phys. Crystallogr.* **274**, 409 (1982).
- ⁸M. I. Bartashevich, A. N. Pirogov, V. I. Voronin, T. Goto, M. Yamaguchi, and I. Yamaguchi, *J. Alloys Compd.* **231**, 104 (1995).
- ⁹J. Liu, D. P. Broom, P. A. L. Georgiev, and D. K. Ross, *J. Alloys Compd.* **356-357**, 174 (2003).
- ¹⁰D. G. Westlake, *J. Less-Common Met.* **75**, 177 (1980).
- ¹¹D. G. Westlake, *J. Less-Common Met.* **90**, 251 (1983).
- ¹²X. Y. Cui, J. Liu, P. A. Georgiev, I. Morrison, D. K. Ross, M. Roberts, K. A. Andersen, M. Telling, and D. Fort, preceding paper, *Phys. Rev. B* **76**, 184443 (2007).
- ¹³A. C. Larson and R. B. Von Dreele, Los Alamos National Laboratory Report No. LAUR 86-748, 2000 (unpublished).
- ¹⁴B. H. Toby, *J. Appl. Crystallogr.* **34**, 210 (2001).
- ¹⁵J. C. Slater, *J. Chem. Phys.* **41**, 3199 (1964).
- ¹⁶D. G. Westlake, *J. Less-Common Met.* **91**, 275 (1983).
- ¹⁷E. Wicke and H. Brodowsky, *Hydrogen in Metals II*, Topics in Applied Physics Vol. 78 (Springer, Berlin, 1978).
- ¹⁸Y. E. Filinchuk and K. Yvon, *J. Solid State Chem.* **179**, 1041 (2006).
- ¹⁹V. F. Sears, *Neutron News* **3** (3), 26 (1992).
- ²⁰L. Néel, *Le Magnetisme* **2**, 79 (1940) (Centre National de la Recherche Scientifique de France, Paris).
- ²¹B. I. Bleaney and B. Bleaney, *Electricity and Magnetism*, 1st ed. (Oxford University Press, New York, 1955), p. 601.
- ²²Y. Mokrousov, G. Bihlmayer, S. Blugel, and S. Heinze, *Phys. Rev. B* **75**, 104413 (2007).
- ²³V. K. Fedotov, V. E. Antonov, I. O. Bashkin, T. Hansen, and I. Natkaniec, *J. Phys.: Condens. Matter* **18**, 1593 (2006).